PNAS RESEARCH ARTICLE | NEUROSCIENCE

Anterior thalamic circuits crucial for working memory

Dheeraj S. Roy[a,1,2], Ying Zhang[b,1,2], Tomomi Aida[b], Chenjie Shen[b], Keith M. Skaggs[b], Yuanyuan Hou[b], Morgan Fleishman[a], Olivia Mosto[b], Alyssa Weninger[b], and Guoping Feng[a,b,2]

Edited by Edward Callaway, Salk Institute for Biological Studies, La Jolla, CA; received October 11, 2021; accepted April 15, 2022

Alterations in the structure and functional connectivity of anterior thalamic nuclei (ATN) have been linked to reduced cognition during aging. However, ATN circuits that contribute to higher cognitive functions remain understudied. We found that the anteroventral (AV) subdivision of ATN is necessary specifically during the maintenance phase of a spatial working memory task. This function engages the AV→parasubiculum (PaS)→entorhinal cortex (EC) circuit. Aged mice showed a deficit in spatial working memory, which was associated with a decrease in the excitability of AV neurons. Activation of AV neurons or the AV→PaS circuit in aged mice was sufficient to rescue their working memory performance. Furthermore, rescued aged mice showed improved behavior-induced neuronal activity in prefrontal cortex (PFC), a critical site for working memory processes. Although the direct activation of PFC neurons in aged mice also rescued their working memory performance, we found that these animals exhibited increased levels of anxiety, which was not the case for AV→PaS circuit manipulations in aged mice. These results suggest that targeting AV thalamus in aging may not only be beneficial for cognitive functions but that this approach may have fewer unintended effects compared to direct PFC manipulations.

working memory | anterior thalamic nuclei | prefrontal cortex | aging | cognitive functions

Significance

Anterior thalamus exhibits significant functional changes with increasing age. While it has been associated with cognitive functions, the specific circuitry relevant for working memory remains unknown. The significance of this study is threefold: First, the anteroventral subdivision of anterior thalamic nuclei is necessary for working memory maintenance; second, aged mice showed a decrease in the excitability of anteroventral thalamic neurons, which correlated with a working memory impairment; and third, activating anteroventral thalamic neurons in aged mice was sufficient to improve their working memory.

Aging is associated with a significant decline in cognitive abilities, including decision-making, memory, visual–spatial integration, and executive functions (1). Although our understanding of the underlying mechanisms of these age-related changes is in its infancy, noninvasive imaging studies in humans have correlated alterations in the shape, volume, and functional connectivity of individual brain regions with cognitive deficits in aging (1–3). One such study reported that decreased functional connectivity of the anterior thalamus, which includes the anterior thalamic nuclei (ATN) complex, along with other cortical regions, contributes to reduced executive functions in older adults (4).

The ATN complex contains dorsal, ventral, and medial subdivisions. These nuclei are part of the cognitive Papez circuit and exhibit connectivity with frontal cortical regions, the hippocampal formation, and hypothalamic nuclei that are involved in a variety of memory functions (5). In rodents, lesion and chemogenetic manipulation studies showed that ATN are crucial for cognitive tasks, such as reference memory, working memory, and spatial navigation (6–11). A recent study in rats with mammillothalamic tract (MTT) lesions showed that optogenetic activation of ATN improved spatial working memory and rhythmic electrical activity, supporting a hub-type role for ATN in the distributed hippocampal–diencephalic–cortical memory network (12). Using fear-learning paradigms, it was found that ATN also contributes to memory encoding and remote memory retrieval (13, 14). While these studies clearly revealed different learning and memory functions of ATN, a causal link between individual ATN circuits and cognitive processes has been lacking (15, 16). We recently developed a transgenic mouse line that provides genetic access to the dorsal subdivision of ATN (i.e., anterodorsal [AD] thalamus) with high specificity (17). Using this line, we showed that distinct ATN projections to the retrosplenial cortex contribute to contextual memory encoding and memory specificity. Further, we demonstrated that the knockdown of several autism and schizophrenia risk genes from AD thalamus leads to cognitive deficits and identified converging cellular mechanisms. While this previous study (17) revealed the physiological role of AD neurons and their dysfunction in some disease states, much less is known about the ventral subdivision of ATN (i.e., anteroventral [AV] thalamus). This is because targeting AV neurons selectively has not been possible using standard circuit-based techniques.

In this study, we wanted to investigate the function of AV thalamus both in adult wild-type mice and aged mice taking advantage of our recently developed Cre line (17) that permits AV-specific labeling. Lesion studies have suggested a particularly important role for AV neurons, among the different ATN subdivisions, in spatial working

Author affiliations: [a]Stanley Center for Psychiatric Research, Broad Institute of Massachusetts Institute of Technology and Harvard University, Cambridge, MA 02142; and [b]McGovern Institute for Brain Research, Department of Brain and Cognitive Sciences, Massachusetts Institute of Technology, Cambridge, MA 02139

Author contributions: D.S.R., Y.Z., and G.F. designed research; D.S.R., Y.Z., T.A., C.S., K.M.S., Y.H., M.F., O.M., and A.W. performed research; D.S.R., Y.Z., and Y.H. performed surgeries; and D.S.R., Y.Z., and G.F. wrote the paper.

The authors declare no competing interest.

This article is a PNAS Direct Submission.

[1]D.S.R. and Y.Z. contributed equally to this work.

[2]To whom correspondence may be addressed. Email: fengg@mit.edu, or droy@broadinstitute.org, or zhangyin@mit.edu.

This article contains supporting information online at http://www.pnas.org/lookup/suppl/doi:10.1073/pnas.2118712119/-/DCSupplemental.

Published May 10, 2022.

memory (15, 16). Given that such experimental approaches were not specific to manipulations of AV thalamus only, and because the circuit mechanism underlying the potential role of AV in working memory remains unknown, here we employed a spatial working memory task. We identified a circuit mechanism by which AV contributes to the maintenance phase of working memory. We also demonstrated that the working memory impairment of aged mice could be rescued by targeting AV neurons. These findings indicate that AV thalamus is not only important for working memory but may serve as a therapeutic target for cognitive disorders.

Results

AV Thalamus Contributes to the Maintenance Phase of Working Memory. We recently developed a C1QL2-Cre mouse line, which in adult animals exhibits strong Cre expression in AD thalamus, dentate gyrus, and retrosplenial cortex (RSC) (17), consistent with the expression pattern of C1QL2 in the adult mouse brain found in the in situ hybridization database generated by the Allen Institute (18). Using C1QL2-Cre mice combined with a CreOff halorhodopsin (NpHR) virus, which enables the expression of NpHR in C1QL2$^-$ neurons, injected in ATN we labeled AV thalamic neurons (Fig. 1 *A*, *Left* and *Middle*). This strategy also led to some weak labeling of anteromedial (AM) neurons (*SI Appendix*, Fig. S1 *A* and *B*). Ex vivo electrophysiological recordings confirmed efficient inhibition of AV neuronal firing in the presence of green light (Fig. 1 *A*, *Right*). To examine spatial working memory, we employed the delayed nonmatch-to-place (DNMP) T-maze protocol and performed phase-specific AV inhibition during the sample, delay (10 s), or choice phases (Fig. 1*B*). Inhibition of AV neurons did not induce changes in locomotion using the open field paradigm, indicating that this manipulation does not lead to alterations in motor behavior that would confound the working memory experiments (Fig. 1*C*). We first trained AV inhibition and control mice in the T-maze task and confirmed that prior to any manipulation both groups showed comparable learning (i.e., days to criterion) (Fig. 1*D*). When we performed AV inhibition in a phase-specific manner, we found that AV thalamus is necessary specifically during the delay phase (effect size d = 1.38 for the NpHR group relative to the eGFP control group) but not the sample or choice phases (Fig. 1*E* and *SI Appendix*, Figs. S1*C* and S3*A*). In these delay phase results, ∼66% of the NpHR group showed comparable or lower levels than the lowest performing eGFP control animal. These observations suggest that AV neurons contribute to the maintenance phase of working memory.

To determine whether this function was specific to AV thalamus, in a different group of animals we labeled AD neurons by injecting Cre-dependent viruses, which permits NpHR expression in C1QL2$^+$ neurons, in the ATN of C1QL2-Cre mice (Fig. 1*F*). In contrast to the role of AV thalamus, inhibition of AD neurons during the sample phase (effect size d = 0.98 for the NpHR group relative to the eYFP control group), but not delay/choice phases, impaired working memory performance (Fig. 1 *G* and *H* and *SI Appendix*, Fig. S3B). In these sample phase results, 50% of the NpHR group showed comparable levels as the lowest performing eYFP control animal. These observations are consistent with our previous study showing a role for AD thalamus in contextual memory encoding (17), and for the first time, reveals differential roles of AD and AV thalamus in a spatial working memory task. We next wanted to quantify the activated neuronal ensembles in AV thalamus during the different behavioral phases. For this purpose, we employed the dual-protein switch system, Cal-Light, which translates neuronal activity–induced calcium signaling into gene expression (i.e., a fluorescent reporter) in a light-dependent manner (19). We injected the Cal-Light viruses in the AV region of wild-type mice and performed behavioral labeling using in vivo phase-specific blue light delivery (Fig. 1*I*). We compared the activated neuronal ensembles labeled with GFP in AV between home cage and the different T-maze phases and found a selective increase during the delay phase (Fig. 1*J*). Consistent with our loss-of-function behavioral observations, these results demonstrate that AV thalamus exhibits an increase in neuronal activity during the maintenance phase of a spatial working memory task.

The AV→Parasubiculum→Entorhinal Cortex Circuit Is Crucial for the Maintenance Phase of Working Memory. To identify the circuit basis for AV's contribution to the maintenance phase of working memory, we performed terminal inhibition experiments by targeting the four major outputs of AV thalamus (5), namely, anterior cingulate cortex (ACC), RSC, presubiculum (PrS), and parasubiculum (PaS). We first validated these projections based on terminal labeling (Fig. 2 *A*, *Top* and *SI Appendix*, Fig. S1 D–I) and using a cFos activation assay to detect increases in postsynaptic neural activity due to AV terminal manipulations (*SI Appendix*, Fig. S1 J–M). Also, cFos activation following terminal light delivery showed that neural activity was modulated in opsin-expressing regions up to ∼500 μm from the optic fiber tip (*SI Appendix*, Fig. S2 A–C). We then carried out delay phase–specific inhibition experiments during the T-maze task. While AV projections to ACC, RSC, and PrS were dispensable for working memory performance, the AV→PaS inhibition group revealed a behavioral deficit (effect size d = 1.09 for the NpHR group relative to the eGFP control group) (Fig. 2 *A*, *Bottom* and *SI Appendix*, Fig. S3 C–E and S4A). Because PaS sends major projections to the entorhinal cortex (EC) (20), a brain region known to participate in spatial working memory (21), we hypothesized that PaS neurons receiving input from AV thalamus and projecting to the EC may underlie working memory maintenance. To test this idea, we injected an anterograde transsynaptic spreading virus expressing Cre (22) in ATN, which labeled downstream target regions with Cre, and injected a Cre-dependent NpHR-eYFP virus in PaS, permitting the labeling of PaS neurons that receive ATN inputs with NpHR-eYFP, followed by optic fiber implants above the EC that targeted PaS terminals (Fig. 2*B* and *SI Appendix*, Figs. S2D and S4B). Optogenetic terminal inhibition in the EC of the ATN→PaS→EC circuit during the delay phase, but not sample or choice phases, impaired working memory performance (effect size d = 1.17 for the NpHR group relative to the eYFP control group) (Fig. 2*C*). In these delay phase results, 50% of the NpHR group showed lower levels than the lowest performing eYFP control animal. Given that AD neurons are not essential during the delay phase of this task, these multicircuit experiments uncovered the neural circuit mechanism by which AV thalamus contributes to the maintenance phase of working memory.

Activating the AV→PaS Circuit Improves Working Memory Performance. While AV thalamus is clearly necessary for working memory, whether increasing AV activity could improve behavioral performance (i.e., gain of function) is not known. In order to consider AV thalamus for potential therapeutic applications, such sufficiency data are critical. We therefore injected

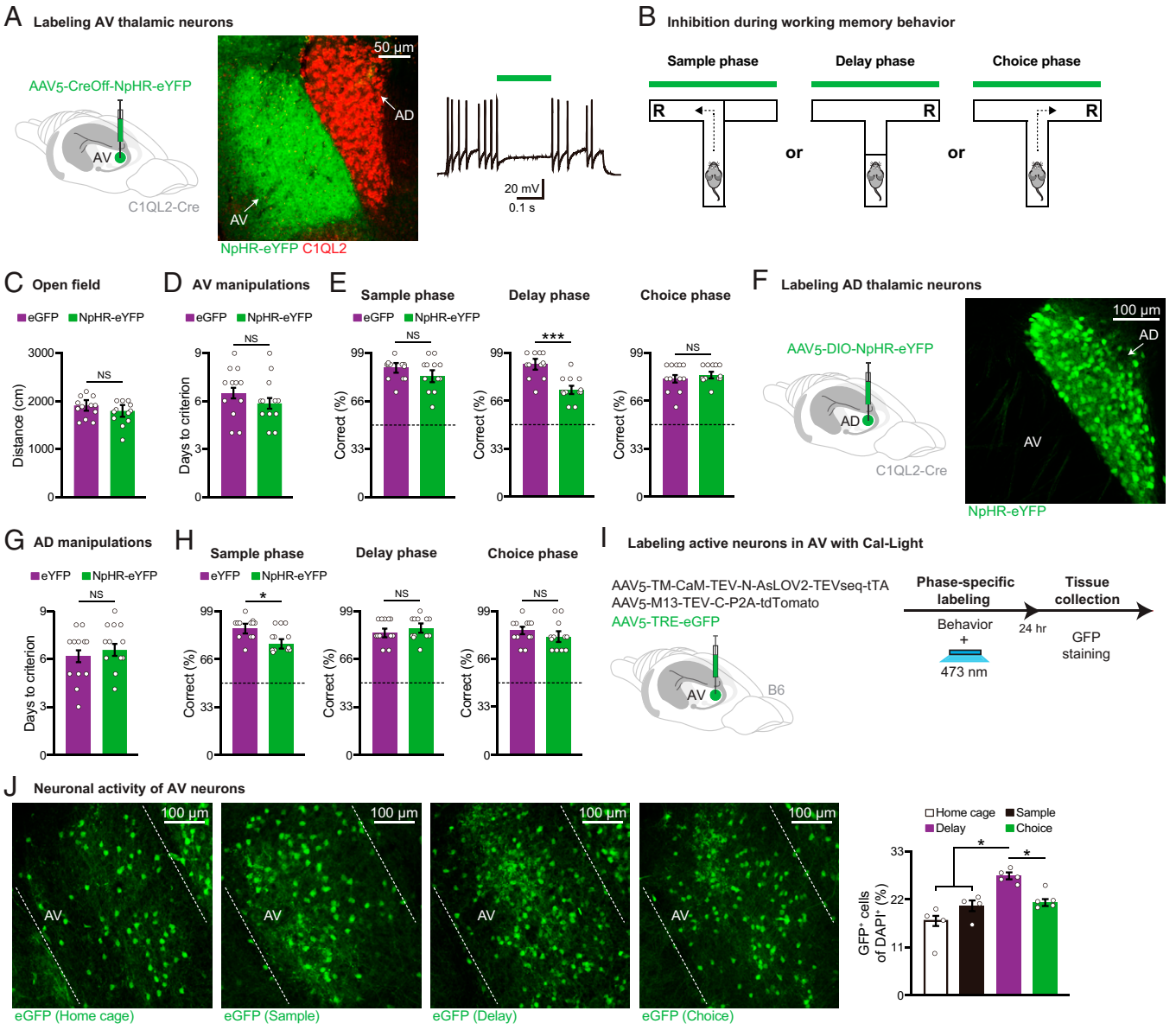

Fig. 1. AV thalamus is crucial for the maintenance phase of working memory. (*A*) Strategy to label AV thalamic neurons by injecting a CreOff-NpHR-eYFP virus in the ATN of C1QL2-Cre mice (*Left*), immunostaining indicates AV labeling with high specificity (C1QL2 is a marker of AD thalamic neurons, *Middle*), ex vivo electrophysiology showing light-induced inhibition of AV neuronal activity (*Right*). (*B*) Inhibition of AV neurons during each of the three different phases in the T-maze paradigm. (*C*) Inhibition of AV during the open field behavioral paradigm. (*D*) Days to criterion before any manipulation. (*E*) Working memory performance for the various phase-specific AV inhibition tests. (*F*) Labeling AD neurons by injecting a DIO-NpHR-eYFP virus in the ATN of C1QL2-Cre mice. (*G*) Days to criterion before any manipulation. (*H*) Working memory performance for the various phase-specific AD inhibition tests. (*I*) We injected a mixture of the three Cal-Light viruses in the AV region for activity-dependent labeling. (*J*) Cal-Light–labeled active neuronal ensembles in AV from home cage, sample phase, delay phase, and choice phase groups (n = 12 mice per group for all behavior panels, n = 4 to 5 mice per group for Cal-Light labeling). Dashed line indicates chance level of performance (i.e., 50% correct choices) in T-maze tests. Data are presented as mean ± SEM; $^{*}P < 0.05$, $^{***}P < 0.001$. Two-tailed unpaired t test (*C*–*E*, *G*, and *H*) and one-way ANOVA followed by Bonferroni post hoc test (*J*).

a CreOff channelrhodopsin (ChR2) virus in the ATN of C1QL2-Cre mice, which labeled C1QL2^{-} neurons with ChR2, combined with optic fiber implants in PaS (Fig. 3 *A*, *Left* and *SI Appendix*, Fig. S4*A*), and validated blue light–induced neuronal firing of AV neurons using ex vivo electrophysiological recordings (Fig. 3 *A*, *Right*). We performed two different circuit activation experiments: One targeting the sample phase and another targeting the delay phase of the T-maze task (Fig. 3*B*). Because the working memory experiments described so far used a 10-s delay period that results in over 85% correct choices in well-trained control mice, we decided to use two additional delay periods (60 s and 90 s) for these activation experiments. Longer delays represent more demanding versions of the T-maze paradigm (17), which would avoid any issues due to a potential ceiling effect in the animals' performance. Focusing on the sample phase-specific activation experiments, although the performance level decreased with longer delay periods, activating the AV→PaS circuit did not modulate behavioral performance (Fig. 3*C*). Strikingly, when we performed AV→PaS circuit activation restricted to the delay phase, working memory performance improved in the 60-s (effect size d = 0.93 for the ChR2 group relative to the mCh control group) and 90-s (effect size d = 1.17 for the ChR2 group relative to the mCh control group) delay tests (Fig. 3*D* and *SI Appendix*, Fig. S2*E*). Together with our previous observations, these data indicated that AV thalamus plays both a necessary and sufficient role in regulating the maintenance phase of working memory.

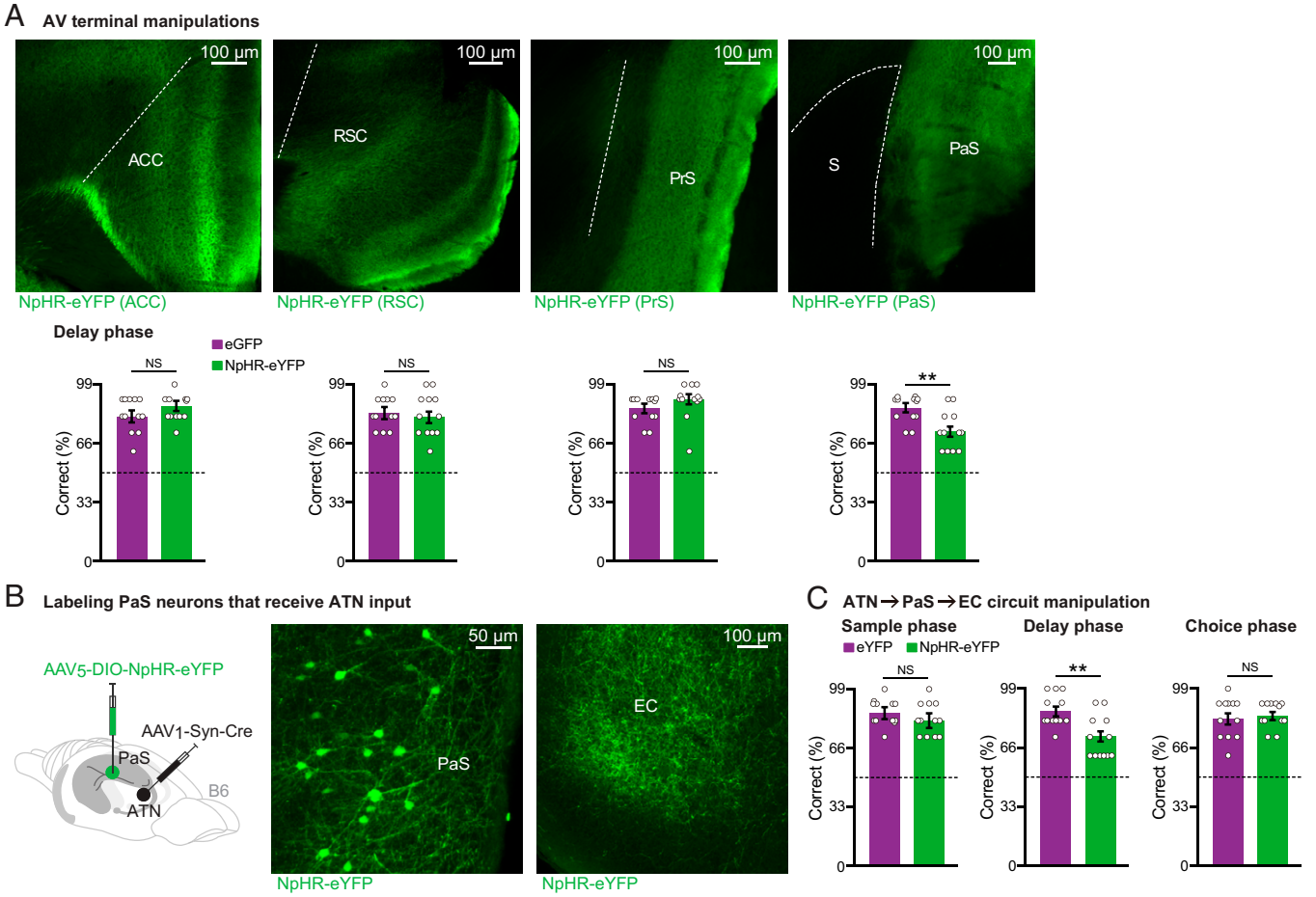

Fig. 2. Identification of AV circuitry recruited during the maintenance phase of working memory. (*A*) Terminal labeling of AV neurons in ACC, RSC, PrS, and PaS (*Top*). S, subiculum. Working memory performance for delay-specific inhibition tests in the different AV terminal groups (*Bottom*). (*B*) By injecting an anterograde Syn-Cre virus in ATN combined with a DIO-NpHR-eYFP virus in PaS, we visualized the ATN→PaS→EC circuit. EC is shown in a coronal section. (*C*) ATN→PaS→EC terminal inhibition during each of the three different phases of the T-maze task (n = 12 mice per group for all behavior panels). Dashed line indicates chance level of performance (i.e., 50% correct choices) in T-maze tests. Data are presented as mean ± SEM; $^{**}P < 0.01$. Two-tailed unpaired t test (*A* and *C*).

Activating AV Thalamus Rescues Working Memory Deficits in Aged Mice. Although human studies have linked anterior thalamic dysfunction to reduced executive functions in older adults (4), age-related alterations in ATN circuits have not been examined. Consistent with previous reports (23), we observed a working memory impairment using a 10-s delay period in 14-mo (aged)- vs. 2-mo-old (young) mice (Fig. 4*A*). Ex vivo electrophysiological recordings revealed a decrease in the neuronal excitability of AV thalamus in aged mice (Fig. 4*B*). Considering our sufficiency behavioral data in adult mice and these physiological observations in aged mice, we hypothesized that activating AV neurons in aged mice may lead to an improvement in their working memory performance. Taking advantage of our previously validated approach (Fig. 3*A*), but this time applying it to aged mice, we found that activating AV neurons during the delay phase in aged mice rescued their working memory (effect size d = 1.02 for the ChR2 group relative to the mCh control group) (Fig. 4*C*). In these AV activation results, 75% of the ChR2 group showed comparable or higher levels than the highest performing mCh control animals. A comparable rescue was achieved when we activated the AV→PaS circuit in 14-mo-old mice (effect size d = 0.90 for the ChR2 group relative to the mCh control group) (Fig. 4*D* and *SI Appendix*, Fig. S4*A*) or 20-mo-old mice (*SI Appendix*, Fig. S2 *F* and G).

To further investigate these rescue observations, we wanted to quantify behavior-induced neuronal activity based on the immediate early gene cFos in prefrontal cortex, which is a critical site for working memory processes (24). As expected, $cFos^+$ neuronal ensembles following T-maze tests were decreased in the PFC of aged mice as compared to young mice (Fig. 4*E*). However, we found that the behavior-induced $cFos^+$ ensembles were significantly increased in aged mice that had received an activation of the AV→PaS circuit during the delay phase (Fig. 4*E*), similar to the effect of AV→PaS activation in young mice (*SI Appendix*, Fig. S2*H*). These observations indicated that activating AV thalamus in aged mice rescues both behavior-induced neuronal activity in the PFC and working memory performance. Because of the correlation between the neuronal activity rescue in the PFC and improved working memory, we wondered whether directly activating PFC neurons may also rescue working memory in aged mice. To test this possibility, we injected a ChR2-expressing virus in the PFC of wild-type mice, which labeled all neurons (Fig. 4*F* and *SI Appendix*, Fig. S4*C*). Indeed, we observed an improvement in the performance of aged mice that received an activation of PFC neurons during the delay phase (Fig. 4*G*). Apart from working memory, the PFC has been linked to a number of other behaviors, including anxiety, fear expression, and reward learning (25). To determine whether direct PFC manipulations may induce other

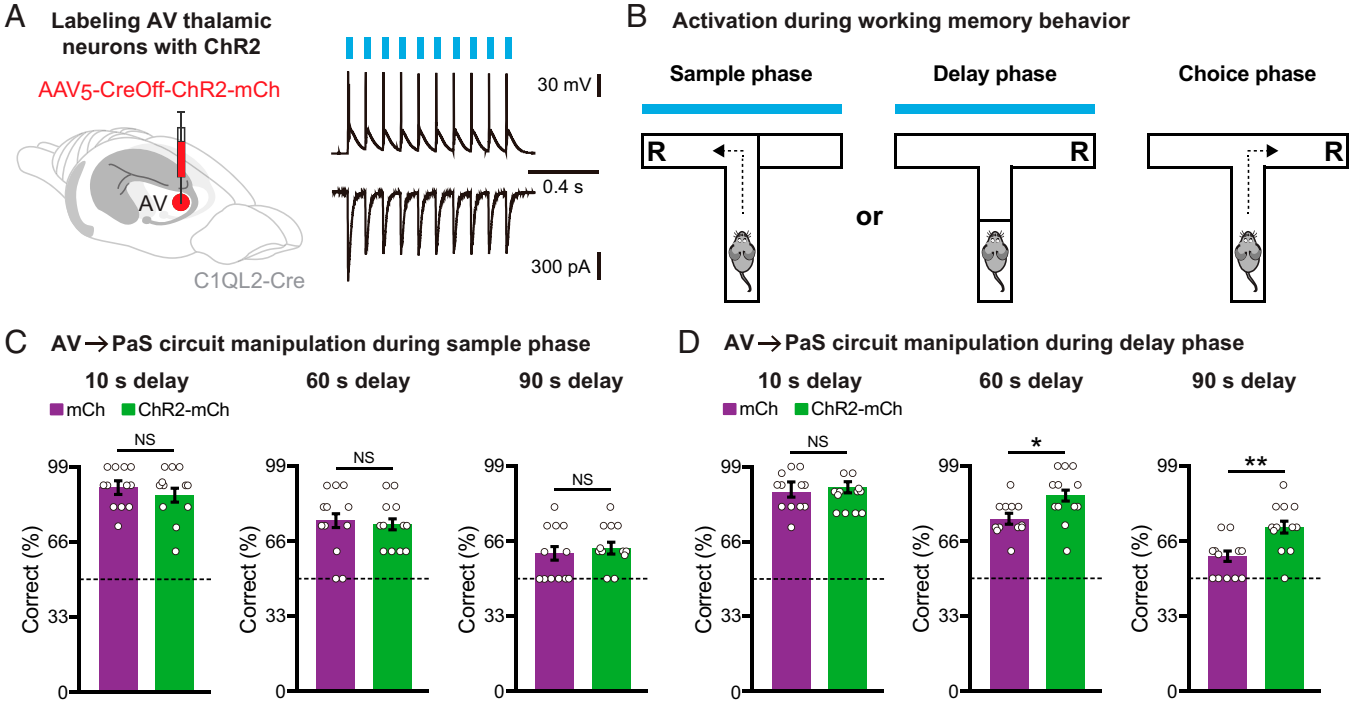

Fig. 3. Activating AV thalamus is sufficient to improve working memory performance. (*A*) Labeling AV neurons by injecting a CreOff-ChR2-mCh virus in the ATN of C1QL2-Cre mice (*Left*), ex vivo electrophysiology showing light-induced activation of AV neurons (*Right*). (*B*) Activation of the AV→PaS circuit during the sample or delay phases in the T-maze paradigm. (*C*) Working memory performance in 10-, 60-, and 90-s delay tests with sample phase-specific AV→PaS circuit activation. (*D*) Working memory performance in 10-, 60-, and 90-s delay tests with delay phase-specific AV→PaS circuit activation (n = 12 mice per group for all behavior panels). Dashed line indicates chance level of performance (i.e., 50% correct choices) in T-maze tests. Data are presented as mean ± SEM; $^{*}P < 0.05$, $^{**}P < 0.01$. Two-tailed unpaired t test (*C* and *D*).

behavioral changes, in addition to rescuing working memory in aged mice, we performed zero maze tests to detect changes in anxiety levels. In contrast to direct PFC manipulations in aged mice, which induced an increase in anxiety levels, AV→PaS circuit manipulations in aged mice exhibited no such alteration in anxiety (Fig. 4*H*). These results suggest that targeting AV thalamus in aging may not only be beneficial for cognitive functions but that this approach may have fewer unintended effects compared to direct PFC manipulations.

Discussion

This study represents a demonstration that the ATN and more specifically the AV thalamus plays a critical role during the maintenance phase of working memory. While we found that AV projections to PaS, a region known to contribute to working memory (26), and subsequently the EC underlie this function, how AV inputs to these regions modulate their neuronal activity specifically during the delay period is an open question. Because it was reported that EC neurons exhibit high-frequency gamma oscillations during the delay period (21), which correlated with a successful execution of working memory behavior, one possibility is that AV thalamus is one of the upstream structures involved in the generation of high-frequency gamma in the EC during this task. Another worthwhile series of experiments should identify inputs to AV neurons that lead to the recruitment of this ATN subdivision during the maintenance phase of working memory. Previous work reported inputs to AV from various subicular regions (27) and RSC (17, 28), which are known to participate in spatial learning and therefore may recruit AV neurons during working memory. It should be noted that in our AV-targeted animals we observed some weak AM thalamus labeling and corresponding subiculum but not PFC terminals. Given the weak nature of these AM terminals combined with their distance away (>500 μm) from the specific optic fiber implant locations, we believe that any potential contribution of AM→subiculum to our AV experiments is minimal. Further, although we believe that the AV→PaS, but not the AV→PrS (i.e., anterior PrS coordinates), circuit is critical for working memory maintenance, because of the close proximity of AV projections to PaS and posterior PrS we cannot rule out some contribution of posterior PrS in our studies.

The mammillary body is another vital source of inputs to ATN neurons through the MTT, which if disrupted, leads to a persistent impairment in spatial working memory (12). Optogenetic ATN stimulation using a 8.5-Hz theta-burst protocol applied throughout the trial is sufficient to improve spatial working memory and enhance rhythmic electrical activity in rats with MTT lesions (12). Using optogenetic inhibition in a behavior phase–specific manner, we revealed the critical role of AV thalamus specifically in the maintenance phase of working memory. It should be noted that we used an abrupt light-off protocol for these optogenetic inhibition experiments, which has been suggested to induce a rebound response immediately following light off. Even though these rebound responses have not been linked to in vivo physiology/behavior changes yet, we cannot rule out a potential effect of such rebounds on our behavioral manipulations. Furthermore, we demonstrated that an activation of AV neurons or the AV→PaS circuit at 20 Hz during the maintenance phase is sufficient to improve working memory in aged mice. Together, our findings extend previous work regarding the role of ATN and their circuits in working memory and support the idea that ATN is a potential therapeutic target for cognitive dysfunction.

Using contextual fear conditioning and cocaine place preference behaviors, we previously showed that AV projections to the RSC contribute to generalization (i.e., memory specificity) (17). Together with our observation that the AV→PaS circuit

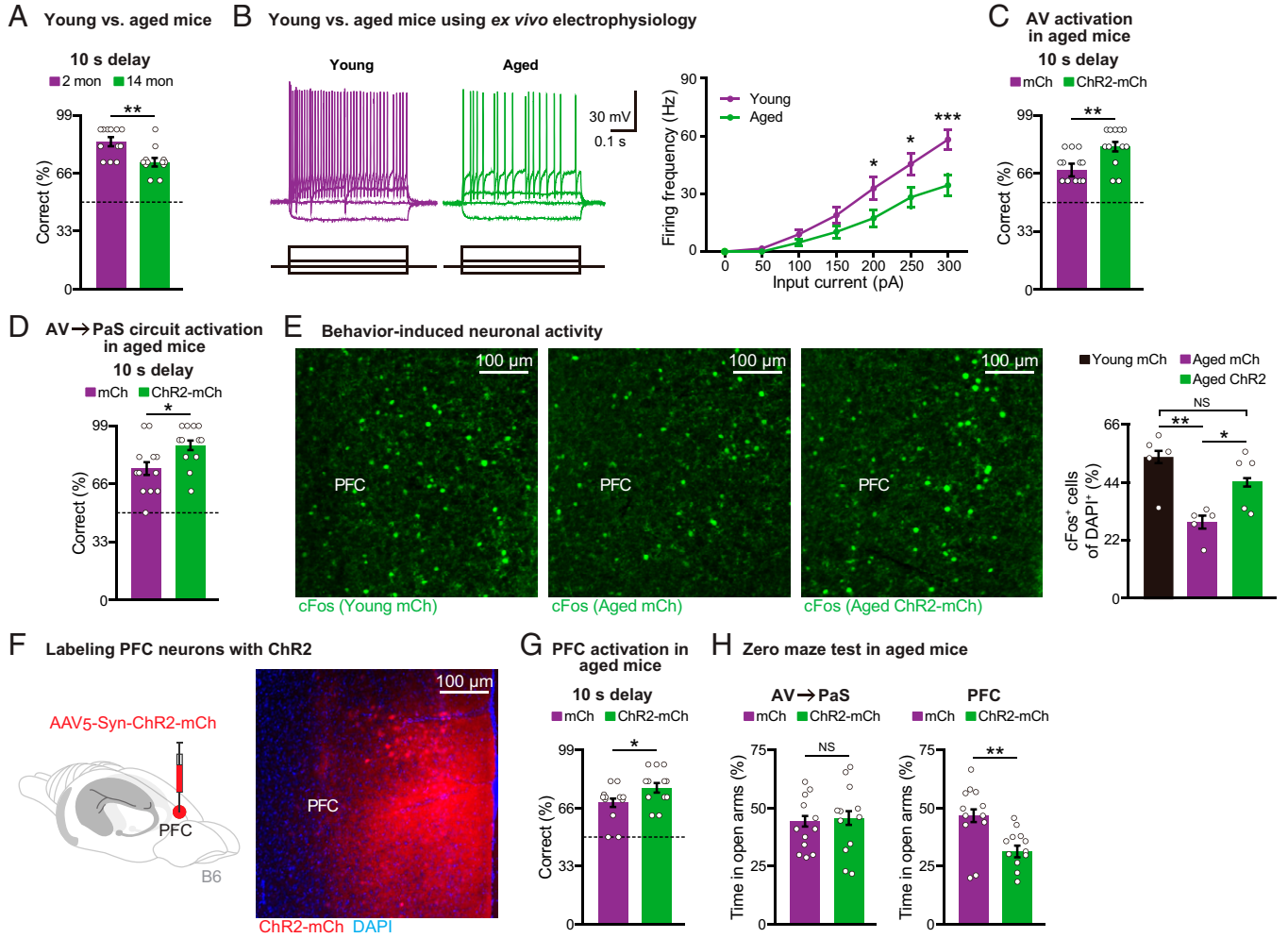

Fig. 4. Targeting AV thalamus rescues working memory deficits in aged mice. (*A*) Working memory performance in young (2 mo) and aged (14 mo) C1QL2-Cre mice. (*B*) Ex vivo electrophysiology showing decreased excitability of AV neurons in aged mice (15 neurons from $n = 3$ young mice, 16 neurons from $n = 3$ aged mice). (*C* and *D*) Activation of AV neurons (*C*) or the AV→PaS circuit (*D*) during the delay period rescues working memory in aged (14 mo old) mice. (*E*) Behavior-induced neuronal activity of prefrontal cortex (PFC) neurons was examined using cFos staining ($n = 5$ mice per group). (*F*) Labeling PFC neurons in wild-type mice with a ChR2-mCh virus. DAPI staining (blue). (*G*) Activation of PFC neurons during the delay period rescues working memory in aged mice. (*H*) Zero maze anxiety test using AV→PaS circuit and PFC neuron activation groups ($n = 12$ mice per group for all behavior panels). Dashed line indicates chance level of performance (i.e., 50% correct choices) in T-maze tests. Data are presented as mean ± SEM; $^*P < 0.05$, $^{**}P < 0.01$, $^{***}P < 0.001$. Two-tailed unpaired *t* test (*A*, *C*, *D*, *G*, and *H*), two-way ANOVA with repeated measures followed by Bonferroni post hoc test (*B*), and one-way ANOVA followed by Bonferroni post hoc test (*E*).

is necessary for working memory, it raises an interesting question: Are the same AV neurons required for both memory specificity and working memory? While this is possible, it could also be the case that distinct AV subpopulations and their circuits have differential functional roles. This functional heterogeneity may map onto the well-known subdivisions within AV thalamus, specifically the anteroventral dorsomedial (AVDM) and anteroventral ventrolateral (AVVL) parts (29, 30), or the anterior–posterior axis as has been shown for other thalamic nuclei (31). Additional work is needed to reveal potential functional heterogeneity (i.e., the presence of thalamic subnetworks) within AV thalamus (32).

Taking advantage of our observation that activating AV thalamic neurons in adult mice is sufficient to improve their working memory performance, we demonstrated that targeting AV thalamus or the AV→PaS circuit in aged mice rescues their working memory impairment. Our data suggest that this behavioral rescue correlates with an improvement in the behavior-induced neuronal activity in the PFC. The significance of these rescue data are that although directly targeting PFC neurons also improved working memory in aged mice, it induced unintended side effects (i.e., changes in anxiety levels), which was not observed when we targeted AV thalamus in aged mice. We therefore propose that AV thalamus may be a therapeutically relevant region for the treatment of working memory impairments. In addition to aging, many brain disorders also lead to cognitive deficits, including Alzheimer's disease (33) and schizophrenia (34). Interestingly, it is known that some schizophrenia patient samples show a decrease in the number of ATN neurons (35). It will be exciting to first determine whether AV thalamic dysfunction is found in animal models of these disorders and subsequently to test whether manipulating AV thalamus can rescue certain cognitive deficits. If so, it would suggest that targeting AV thalamus may be applicable to a range of different disorders that exhibit cognitive deficits. Regarding translational approaches, while we employed optogenetics to activate AV neurons in vivo, future studies should identify molecular targets capable of modulating AV thalamus that would be compatible with noninvasive therapeutic strategies. In conclusion, this work provides a better understanding of how ATN contributes to working memory and consistent with our previous study (17) revealed a link between ATN dysfunction and cognitive impairments in aging.

Materials and Methods

Mice. C1QL2-IRES-Cre knockin mice were generated using cloning-free CRISPR as previously described (17). Briefly, a C1QL2-IRES-Cre targeting vector was constructed by Gibson assembly using an IRES-Cre-pA cassette (a kind gift from Z. Josh Huang, Cold Spring Harbor Laboratory, Cold Spring Harbor, NY), PCR-amplified 2-kb C1QL2 homology arms, and a pBluescript plasmid backbone. Injection mixtures were prepared by mixing crRNA (CGCCCUCUAGGCCCCUAAUC for protospacer sequence) and tracrRNA. The mixture was heat denatured, followed by reannealing at room temperature. EnGen Cas9 NLS, *Streptococcus pyogenes* was added, and the mixture was incubated at 37 °C for 15 min, then mixed with the C1QL2-IRES-Cre targeting vector. Pronuclear microinjections in zygotes were performed using 1 to 2 pL of the injection mixture. Following injections, embryos were surgically implanted into pseudopregnant CD-1 females and allowed to develop normally until natural birth. Genomic DNA was purified from tail samples and PCR genotyped. Cre mice were maintained as hemizygotes. C57BL/6J wild-type (or B6) mice were obtained from The Jackson Laboratory. All mice used in this study were males, between the ages of 8 and 12 wk at the time of surgery. One exception was for aged mice experiments, which employed 14-mo-old animals. Mice had access to food and water ad libitum and were socially housed in numbers of two to five littermates until surgery. Following surgery, mice were single housed. All experiments were conducted in accordance with NIH guidelines and the Massachusetts Institute of Technology, Department of Comparative Medicine, and the committee on animal care.

Viral Constructs. The following CreOff (DO) AAV constructs were acquired from Addgene: AAV-EF1α-DO-NpHR3.0-eYFP (plasmid No. 37087), AAV-EF1α-DO-eGFP (plasmid No. 37085), AAV-EF1α-DO-ChR2-mCherry (plasmid No. 37082), and AAV-EF1α-DO-mCherry (plasmid No. 37119). The Cal-Light AAV constructs were also acquired from Addgene: AAV-TM-CaM-TEV-N-AsLOV2-TEVseq-tTA (plasmid No. 92392), AAV-M13-TEV-C-P2A-tdTomato (plasmid No. 92391), and AAV-TRE-eGFP (plasmid No. 89875). All these plasmids were serotyped with AAV_5 coat proteins and packaged by the viral core at Boston Children's Hospital (~2×10^{13} GC mL^{-1} viral titers). The following viruses were acquired from Addgene: AAV_5-EF1α-DIO-NpHR3.0-eYFP (catalog No. 26966-AAV_5, 7×10^{12} GC mL^{-1} titer), AAV_1-Syn-Cre (anterograde virus, catalog No. 105553-AAV_1, 1×10^{13} GC mL^{-1} titer), and AAV_5-Syn-ChR2-mCherry (catalog No. 26976-AAV_5, 7×10^{12} GC mL^{-1} titer). The AAV_5-EF1α-DIO-eYFP virus (1.2×10^{13} GC mL^{-1} viral titer) was acquired from the University of North Carolina at Chapel Hill Vector Core.

Mouse Surgery and Optic Fiber Implants. Animals were anesthetized with isoflurane for stereotaxic injections and given 1 mg kg^{-1} meloxicam as an analgesic prior to incisions. Injections were targeted to AV (−0.58 mm anterior-posterior [AP], ±0.95 mm medial-lateral [ML], −3.25 mm dorsal-ventral [DV]), AD (−0.7 mm AP, ±0.65 mm ML, −2.75 mm DV), ATN (−0.55 mm AP, ±0.9 mm ML, −3.15 mm DV), PaS (−4.3 mm AP, ±2.4 mm ML, −3.9 mm DV), and PFC (+2.0 mm AP, ±0.2 mm ML, −2.4 mm DV). For behavioral manipulation and Cal-Light experiments using optogenetics, single monofiber implants (200-μm core diameter, numerical aperture [NA] 0.22, NewDoon) were lowered above the injection sites for AV/AD bilaterally (i.e., based on DV coordinates, 0.15 mm closer to the surface of the brain; fiber length for AD was 3 mm; for AV, 3.5 mm). For terminal manipulation experiments, bilateral monofiber implants (200-μm core diameter, NA 0.22, NewDoon) were targeted to the ACC (+1.0 mm AP, ±1.0 mm ML, −2.0 mm DV), RSC (−2.46 mm AP, ±0.25 mm ML, −0.9 mm DV), PrS (−4.0 mm AP, ±2.0 mm ML, −2.2 mm DV), PaS (coordinates listed above), and EC (−4.75 mm AP, ±3.5 mm ML, −3.7 mm DV). Fiber length for RSC was 1 mm; for ACC/PrS, 2.5 mm; and for PaS/EC, 4 mm. Injection volumes across injection sites were 250 nL each. To identify the spread of the AAV_1-Syn-Cre virus in the ATN, we mixed this virus with Dil555 (catalog No. 60010, Biotium) in a 1:1 mixture immediately prior to surgeries. Viruses were injected at 70 nL min^{-1} using a glass micropipette attached to a 10-mL Hamilton microsyringe. The needle was lowered to the target site and remained for 5 min before beginning the injection. After the injection, the needle stayed for 10 min before it was withdrawn. Implants were secured to the skull with two jewelry screws, adhesive cement (C&B Metabond), and dental cement. Mice were given 1 to 2 mg kg^{-1} sustained-release buprenorphine as analgesic after surgeries and allowed to recover for at least 2 wk before behavioral experiments. All injection sites were verified histologically. As criteria, we only included mice with virus expression limited to the targeted regions. Specifically, for AV-targeted animals, we only included mice in which strong AV labeling was observed along with minimal AM labeling (i.e., less than 5% labeling of AM thalamus based on fluorescent intensity) as well as no labeling in mediodorsal/paraventricular nuclei. For AD-targeted animals, we only included mice in which strong AD labeling was observed. For terminal manipulation studies, we only included mice in which fluorescent labeling was confirmed in the target region along with optic fiber tracks. For PFC-targeted animals, we only included mice in which strong PFC labeling was observed without any neighboring anterior cingulate cortex labeling.

Immunohistochemistry. Mice were dispatched using an overdose of isoflurane and transcardially perfused with phosphate buffered saline (PBS), followed by 4% paraformaldehyde (PFA). Brains were extracted and incubated in 4% PFA at room temperature overnight. Brains were transferred to PBS, and 50-μm coronal slices were prepared using a vibratome. For immunostaining, each slice was placed in PBS + 0.2% Triton X-100 (PBS-T), with 5% normal goat serum for 1 h and then incubated with primary antibody at 4 °C for 24 h. Slices then underwent three wash steps for 10 min each in PBS-T, followed by a 2-h incubation with secondary antibody. After three more wash steps of 10 min each in PBS-T, slices were mounted on microscope slides. Antibodies used for staining were as follows: Rabbit anti-C1QL2 (1:500; catalog No. PA5-101536, Thermo Fisher) and anti-rabbit Alexa-555 (1:500; catalog No. A27039, Invitrogen), chicken anti-GFP (1:1,000; catalog No. A11122, Invitrogen), anti-chicken Alexa-488 (1:1,000; catalog No. A11039, Invitrogen), rabbit anti-cFos (1:500; catalog No. 2250, Cell Signaling Technology), and anti-rabbit Alexa-488 (1:300; catalog No. A11008, Invitrogen), and nuclei were stained with DAPI (1:3,000, Sigma). Across group staining experiments were performed blind to the specific manipulation/group information.

Optogenetic Experiments. For optogenetic neuronal activity manipulation experiments, NpHR was activated with a 570-nm laser (10 mW, constant green light) and immediately turned off at the end of the target epoch. Cal-Light was activated with a 473-nm laser (8 to 10 mW, constant blue light) and ChR2 was activated at 12 or 20 Hz (15-ms pulse width) with a 473-nm laser (10 to 15 mW, blue light).

Cell Counting. Brain sections were imaged with a 20× magnification objective on a Leica confocal microscope. Images were processed using ImageJ, and quantifications were performed manually from three to five sections per animal. All counting experiments were conducted blind to experimental group. Researcher 1 trained the animals, prepared slices, and randomized images, while researcher 2 performed cell counting. For Cal-Light experiments, percentage of GFP^+ cells in AV among $DAPI^+$ cells was calculated as $(GFP^+/DAPI^+) \times 100$. To quantify the number of activated ($cFos^+$) neurons in the PFC across behavioral groups, percentage of $cFos^+$ cells among $DAPI^+$ cells was calculated as $(cFos^+/DAPI^+) \times 100$. Data were analyzed using Microsoft Excel with the Statplus plug-in or Prism 6 software.

Ex Vivo Electrophysiology.

Slice preparation. Across group ex vivo recordings were conducted blind to the specific manipulation/group information. Researcher 1 prepared the animals, while researcher 2 dispatched the animals and conducted physiological recordings. Mice (8 to 12 wk or 14 mo old) were anesthetized with isoflurane, decapitated, and brains were quickly removed. Brains were placed in ice-cold artificial cerebrospinal fluid (ACSF) consisting of (in millimoles): 125 NaCl, 3 KCl, 1.25 NaH_2PO_4, 2 $MgSO_4$, 2 $CaCl_2$, 25 $NaHCO_3$, and 10 D-glucose. Coronal slices (300 μm thick) were prepared in an oxygenated cutting solution at 4 °C by using a vibratome (Leica). The cutting solution contained (in millimoles): 30 NaCl, 4.5 KCl, 1.2 NaH_2PO_4, 194 sucrose, 26 $NaHCO_3$, 10 D-glucose, 0.2 $CaCl_2$, 8 $MgSO_4$, and saturated with 95% O_2–5% CO_2 (pH 7.3, osmolarity of 350 mOsm). Slices were recovered in ACSF at 33 °C (±0.5 °C) for 30 min and then kept at room temperature until recording. The ACSF contained (in millimoles): 119 NaCl, 2.3 KCl, 2.5 $CaCl_2$, 1.3 $MgSO_4$, 26.2 $NaHCO_3$, 1 NaH_2PO_4, 11 D-glucose, and saturated with 95% O_2–5% CO_2 (pH 7.3, osmolarity of 300 mOsm).

Electrophysiological recordings. Whole cell recordings in current-clamp or voltage-clamp mode were performed using an infrared-differential interference

contrast (IR-DIC) microscope (Olympus) with a water immersion 40× objective (NA 0.8), equipped with four automatic manipulators (Luigs & Neumann) and a charge coupled device (CCD) camera (Hamamatsu Co). For all recordings, borosilicate glass pipettes were fabricated (Sutter Instrument) with resistances of 3.5 to 5 MΩ. Voltage clamp recordings were performed using the following intracellular solution (in millimoles): 120 cesium methansulfonate, 10 Hepes, 1.1 ethylene glycol-bis(β-aminoethyl ether)-*N*,*N*,*N*′,*N*′-tetraacetic acid (EGTA), 5 NaCl, 1.1 TEA-Cl, 4 Mg-adenosine triphosphate (ATP), 0.3 Na-guanosine 5' triphosphate (GTP), 4 QX314, and 0.5% biocytin. The osmolarity of this intracellular solution was 298 mOsm and the pH was 7.2. Neurons were held at −80 mV and stepped from −60 mV to +20 mV in 10-mV increments, in the presence of tetrodotoxin (TTX) (1 μM), picrotoxin (100 μM), 4AP (1 mM), tetraethylammonium chloride (10 mM), and cesium chloride (2 mM). For other recordings, pipettes were filled with the following intracellular solution (in millimoles): 110 K-gluconate, 40 KCl, 10 Hepes, 3 ATP, 0.5 GTP, 0.2 EGTA, and 0.5% biocytin. The osmolarity of this intracellular solution was 290 mOsm and the pH was 7.25. A series of 500-ms suprathreshold currents of 50 to 300 pA were used to quantify the excitability with holding at −55 mV. Recordings were amplified using up to two dual channel amplifiers (Molecular Devices), filtered at 2 kHz, digitized (20 kHz), and acquired through an analog to digital converter/digital to analog converter data acquisition unit (InstruTech) using custom software running on Igor Pro (Wavemetrics). Access resistance (RA) was monitored throughout the duration of the experiment and data acquisition was suspended whenever RA was beyond 20 MΩ.

Optogenetic stimulation during recordings. Optogenetic stimulation was achieved through Polygon400 (Mightex) with built-in light-emitting diode sources (470 or 570 nm). Light power on the sample was 20 mW/mm^2. To test ChR2 expression, slices were stimulated with 5- or 20-Hz blue light pulses. To test NpHR function, continuous green light was delivered to the slices.

Post hoc immunohistochemistry. Recorded cells were filled with biocytin and subsequently recovered for brain region/cell type verification. Slices were first incubated with 4% PFA for 16 h at 4 °C. After washing with 0.5% Triton X-100 in PBS, slices were incubated in 5% normal goat serum for 2 h. Following serum, slices were incubated in streptavidin CF555 (1:200; catalog No. 92214, Biotium) for 2 h at room temperature. Before mounting, slices were incubated with DAPI (1:3,000; Sigma) for 30 min.

Behavior Assays. Experiments were conducted during the light cycle (7 AM to 7 PM). Mice were randomly assigned to experimental groups for specific behavioral assays. Mice were habituated to investigator handling for 1 to 2 min on 3 consecutive days. Handling took place in the holding room where the mice were housed. Prior to each handling session, mice were transported by wheeled cart to and from the vicinity of the behavior rooms to habituate them to the journey. All behavior experiments were analyzed blind to experimental group. Given behavioral variability, assays were performed using a minimum of 12 mice per group to ensure adequate power for any observed differences, which were run in two batches of 6 mice each to confirm reproducibility of various phenotypes.

Open field exploration. Spontaneous motor activity was measured in an open field arena (40 × 40 × 30 cm) for 10 min. Mice were transferred to the testing room and acclimated for 30 min before the test session. During the testing period, standard lighting in the room was replaced with an adjustable light source to achieve 60 lx within the open field arena. The apparatus was cleaned with quatricide before and between runs. Total movement (distance traveled) in the arena was quantified using an automated infrared detection system (Omnitech Digiscan, AccuScan Instruments). To test the effect of optogenetic manipulations on locomotion, mice were plugged into the laser source and light was turned on once the animals were placed into the arena. Raw data were extracted and analyzed using Microsoft Excel.

Spatial working memory: T maze. For spatial working memory behavior, we used the DNMP T-maze protocol. Mice selected for this paradigm were food deprived until they reached 85% of their initial body weight. During food deprivation, mice were habituated to sugar pellets (20 mg), which would subsequently be used as a reward in the T maze. The behavioral chamber was located in a 5 × 4.8 m room, which did not have any windows, but had other spatial cues (e.g., table, laptop, shelves, transportation cart). Lighting of ∼120 lx was used during behavioral experiments. Prior to bringing the test animals using a transportation cart to the room, sugar pellets were placed in cups outside but right next to the behavioral chamber out of the animal's sight to control for potential odor cues. Mice were habituated to the T maze for 10 min. During habituation to the maze, sugar pellet rewards were placed in the reward cups (2.5-cm diameter) at the end of each arm, and replaced as they were consumed. The behavioral training consisted of 10 trials per day with each trial having two separate runs (sample and choice runs). The first run in each trial was the sample run, in which mice were placed in the stem of the T maze and allowed to run to the end of one arm of the maze (the other arm was closed off). This open arm was rewarded. After reward consumption, mice were returned to their home cage for ∼30 s when the T maze was quickly cleaned and both arms were opened. Mice were once again placed in the stem of the T maze and during this choice run mice were allowed to choose which of the two arms to visit. The opposite arm from the one visited during the previous sample run was rewarded. If the mouse chose the incorrect arm (i.e., the previous arm), it was blocked in that arm for a 30-s punishment. Following this sample and choice run procedure for a single trial, each mouse performed 9 more trials per day with an intertrial interval of 20 min. Mice were manually scored on the percentage of time that they made a successful alternation and how many days until they reached a daily success rate of over 70% for 2 consecutive days (referred to as days to criterion). Once they reached criterion, the next 2 days were used for testing animals' success rate when the delay between sample and choice runs was 10 s (10 trials per day). Their performance in the 10-s delay condition was an average of these 2 test days. Similarly, the following 2 days were used for testing animals' success rate when the delay between sample and choice runs was 60 s (10 trials per day). This was repeated for 90-s delay conditions. Optogenetic manipulations were restricted to the sample, delay, or choice phases. For Cal-Light experiments, a 60-s delay period was used over 10 trials in order to obtain sufficient levels of activated neuronal ensembles, as revealed by post hoc GFP staining.

Zero maze test. The elevated zero maze apparatus had four equally divided quadrants, specifically two open and two closed arms, and the setup was elevated ∼2.5 ft above the floor. Using indirect lighting, the open arms were at 60 lx and the closed arms were at 10 lx. Mice were placed in the center of a closed arm and allowed to explore the arena for 5 min. Animal placement was counterbalanced. The relative time spent in the closed arms was used as an expression of anxiety-like behavior. These experiments were performed with optogenetic manipulations for the entire 5-min window. Automated analysis was performed using Noldus Observer software.

Statistical Analysis. All data analyses were conducted blind to experimental groups. The number of replicates (n) is indicated in the figure legends and refers to the number of experimental subjects independently treated in each experimental condition. Data are presented as mean values accompanied by SEM. Statistical comparisons were performed using Microsoft Excel with the Statplus plug-in, Python, and Prism 6 software. One-way ANOVA followed by Bonferroni post hoc tests, two-way ANOVA with repeated measures followed by Bonferroni post hoc tests, and two-tailed unpaired t tests were used to test for statistical significance when appropriate. No statistical methods were used to predetermine sample sizes. Statistical significance threshold was set at $\alpha = 0.05$ (not significant [NS], $P > 0.05$; *$P < 0.05$; **$P < 0.01$; ***$P < 0.001$).

Data Availability. Individual mouse data for all behavior, cell counting, and electrophysiology experiments are available within the submitted materials. The C1QL2-Cre mouse line has been approved for deposit by The Jackson Laboratory (strain No. 36955). All other study data are included in the article and/or supporting information.

ACKNOWLEDGMENTS. We thank C. Wang for viral packaging, H. Zaniewski for experimental assistance, and all members of the G.F. laboratory for their support. D.S.R. was supported by the Warren Alpert Distinguished Scholar Award and NIH 1K99NS125121-01. Y. Z. was supported by the J. Douglas Tan Fellowship. T.A. was supported by MEXT (Grant-in-Aid for Scientific Research 816K07085), Center for Novel Science Initiatives/National Institutes of Natural Sciences (BS281001), the Nakatani Foundation, the SENSHIN Medical Research Foundation, the Mochida Memorial Foundation, the Takeda Science Foundation, the Medical Research Institute of Tokyo Medical and Dental University (TMDU), and the TMDU President Award. This work was supported by the Stanley Center for Psychiatric Research at the Broad Institute of Massachusetts Institute of Technology (MIT) and Harvard University, the Hock E. Tan and K. Lisa Yang Center for Autism Research at MIT, and the James and Patricia Poitras Center for Psychiatric Disorders Research at MIT (to G.F.).

1. C. N. Harada, M. C. Natelson Love, K. L. Triebel, Normal cognitive aging. *Clin. Geriatr. Med.* **29**, 737–752 (2013).
2. D. L. Murman, The impact of age on cognition. *Semin. Hear.* **36**, 111–121 (2015).
3. E. J. Hughes *et al.*, Regional changes in thalamic shape and volume with increasing age. *Neuroimage* **63**, 1134–1142 (2012).
4. S. M. Grieve, L. M. Williams, R. H. Paul, C. R. Clark, E. Gordon, Cognitive aging, executive function, and fractional anisotropy: A diffusion tensor MR imaging study. *AJNR Am. J. Neuroradiol.* **28**, 226–235 (2007).
5. M. M. Jankowski *et al.*, The anterior thalamus provides a subcortical circuit supporting memory and spatial navigation. *Front. Syst. Neurosci.* **7**, 45 (2013).
6. J. P. Aggleton, A. B. Keith, A. Sahgal, Both fornix and anterior thalamic, but not mammillary, lesions disrupt delayed non-matching-to-position memory in rats. *Behav. Brain Res.* **44**, 151–161 (1991).
7. E. C. Warburton, J. P. Aggleton, Differential deficits in the Morris water maze following cytotoxic lesions of the anterior thalamus and fornix transection. *Behav. Brain Res.* **98**, 27–38 (1999).
8. A. S. Mitchell, J. C. Dalrymple-Alford, Lateral and anterior thalamic lesions impair independent memory systems. *Learn. Mem.* **13**, 388–396 (2006).
9. L. M. Savage, J. M. Hall, R. P. Vetreno, Anterior thalamic lesions alter both hippocampal-dependent behavior and hippocampal acetylcholine release in the rat. *Learn. Mem.* **18**, 751–758 (2011).
10. S. S. Winter, B. J. Clark, J. S. Taube, Spatial navigation. Disruption of the head direction cell network impairs the parahippocampal grid cell signal. *Science* **347**, 870–874 (2015).
11. A. J. D. Nelson, L. Kinnavane, E. Amin, S. M. O'Mara, J. P. Aggleton, Deconstructing the direct reciprocal hippocampal-anterior thalamic pathways for spatial learning. *J. Neurosci.* **40**, 6978–6990 (2020).
12. S. C. Barnett *et al.*, Anterior thalamic nuclei neurons sustain memory. *CRNEUR* **2**, 100022 (2021).
13. N. Yamawaki *et al.*, Long-range inhibitory intersection of a retrosplenial thalamocortical circuit by apical tuft-targeting CA1 neurons. *Nat. Neurosci.* **22**, 618–626 (2019).
14. G. Vetere *et al.*, An inhibitory hippocampal-thalamic pathway modulates remote memory retrieval. *Nat. Neurosci.* **24**, 685–693 (2021).
15. J. P. Aggleton, P. R. Hunt, S. Nagle, N. Neave, The effects of selective lesions within the anterior thalamic nuclei on spatial memory in the rat. *Behav. Brain Res.* **81**, 189–198 (1996).
16. G. Byatt, J. C. Dalrymple-Alford, Both anteromedial and anteroventral thalamic lesions impair radial-maze learning in rats. *Behav. Neurosci.* **110**, 1335–1348 (1996).
17. D. S. Roy *et al.*, Anterior thalamic dysfunction underlies cognitive deficits in a subset of neuropsychiatric disease models. *Neuron* **109**, 2590–2603.e13 (2021).
18. E. S. Lein *et al.*, Genome-wide atlas of gene expression in the adult mouse brain. *Nature* **445**, 168–176 (2007).
19. D. Lee, J. H. Hyun, K. Jung, P. Hannan, H. B. Kwon, A calcium- and light-gated switch to induce gene expression in activated neurons. *Nat. Biotechnol.* **35**, 858–863 (2017).
20. M. Caballero-Bleda, M. P. Witter, Regional and laminar organization of projections from the presubiculum and parasubiculum to the entorhinal cortex: An anterograde tracing study in the rat. *J. Comp. Neurol.* **328**, 115–129 (1993).
21. J. Yamamoto, J. Suh, D. Takeuchi, S. Tonegawa, Successful execution of working memory linked to synchronized high-frequency gamma oscillations. *Cell* **157**, 845–857 (2014).
22. B. Zingg *et al.*, AAV-mediated anterograde transsynaptic tagging: Mapping corticocollicular input-defined neural pathways for defense behaviors. *Neuron* **93**, 33–47 (2017).
23. J. L. Bizon, T. C. Foster, G. E. Alexander, E. L. Glisky, Characterizing cognitive aging of working memory and executive function in animal models. *Front. Aging Neurosci.* **4**, 19 (2012).
24. A. H. Lara, J. D. Wallis, The role of prefrontal cortex in working memory: A mini review. *Front. Syst. Neurosci.* **9**, 173 (2015).
25. R. J. Davidson, Anxiety and affective style: Role of prefrontal cortex and amygdala. *Biol. Psychiatry* **51**, 68–80 (2002).
26. R. P. Kesner, R. Giles, Neural circuit analysis of spatial working memory: Role of pre- and parasubiculum, medial and lateral entorhinal cortex. *Hippocampus* **8**, 416–423 (1998).
27. N. F. Wright, J. T. Erichsen, S. D. Vann, S. M. O'Mara, J. P. Aggleton, Parallel but separate inputs from limbic cortices to the mammillary bodies and anterior thalamic nuclei in the rat. *J. Comp. Neurol.* **518**, 2334–2354 (2010).
28. H. Shibata, J. Naito, Organization of anterior cingulate and frontal cortical projections to the anterior and laterodorsal thalamic nuclei in the rat. *Brain Res.* **1059**, 93–103 (2005).
29. R. P. Vertes, S. B. Linley, H. J. Groenewegen, M. P. Witter, "Thalamus" in *The Rat Nervous System*, G. Paxinos, Ed. (Academic Press, 2015), pp. 336–365.
30. E. Lomi *et al.*, Evidence for two distinct thalamocortical circuits in retrosplenial cortex. *Neurobiol. Learn. Mem.* **185**, 107525 (2021).
31. C. Gao *et al.*, Two genetically, anatomically and functionally distinct cell types segregate across anteroposterior axis of paraventricular thalamus. *Nat. Neurosci.* **23**, 217–228 (2020).
32. D. S. Roy, Y. Zhang, M. M. Halassa, G. Feng, Thalamic subnetworks as units of function. *Nat. Neurosci.* **25**, 140–153 (2022).
33. A. D. Baddeley, S. Bressi, S. Della Sala, R. Logie, H. Spinnler, The decline of working memory in Alzheimer's disease. A longitudinal study. *Brain* **114**, 2521–2542 (1991).
34. T. A. Lett, A. N. Voineskos, J. L. Kennedy, B. Levine, Z. J. Daskalakis, Treating working memory deficits in schizophrenia: A review of the neurobiology. *Biol. Psychiatry* **75**, 361–370 (2014).
35. K. A. Young, K. F. Manaye, C. Liang, P. B. Hicks, D. C. German, Reduced number of mediodorsal and anterior thalamic neurons in schizophrenia. *Biol. Psychiatry* **47**, 944–953 (2000).